Published online 15 April 2019

Nucleic Acids Research, 2019, Vol. 47, No. 13 ***e75***
doi: 10.1093/nar/gkz271

Cell-specific CRISPR–Cas9 activation by microRNA-dependent expression of anti-CRISPR proteins

Mareike D. Hoffmann[1,2], Sabine Aschenbrenner[1,2], Stefanie Grosse[1], Kleopatra Rapti[3,4], Claire Domenger[3,4], Julia Fakhiri[3,4], Manuel Mastel[1], Kathleen Börner[3,4,5], Roland Eils[6,7,*], Dirk Grimm[3,4,5,*] and Dominik Niopek[1,*]

[1]Synthetic Biology Group, Institute for Pharmacy and Biotechnology (IPMB) and Center for Quantitative Analysis of Molecular and Cellular Biosystems (BioQuant), University of Heidelberg, Heidelberg 69120, Germany, [2]Division of Theoretical Bioinformatics, German Cancer Research Center (DKFZ), Heidelberg 69120, Germany, [3]Department of Infectious Diseases, Virology, University Hospital Heidelberg, Heidelberg 69120, Germany, [4]BioQuant Center and Cluster of Excellence CellNetworks at Heidelberg University, Heidelberg 69120, Germany, [5]German Center for Infection Research (DZIF), partner site Heidelberg, Heidelberg 69120, Germany, [6]Digital Health Center, Berlin Institute of Health (BIH) and Charité, Berlin 10178, Germany and [7]Health Data Science Unit, University Hospital Heidelberg, Heidelberg 69120, Germany

Received November 27, 2018; Revised April 01, 2019; Editorial Decision April 03, 2019; Accepted April 05, 2019

ABSTRACT

The rapid development of CRISPR–Cas technologies brought a personalized and targeted treatment of genetic disorders into closer reach. To render CRISPR-based therapies precise and safe, strategies to confine the activity of Cas(9) to selected cells and tissues are highly desired. Here, we developed a cell type-specific Cas-ON switch based on miRNA-regulated expression of anti-CRISPR (Acr) proteins. We inserted target sites for miR-122 or miR-1, which are abundant specifically in liver and cardiac muscle cells, respectively, into the 3′UTR of Acr transgenes. Co-expressing these with Cas9 and sgRNAs resulted in Acr knockdown and released Cas9 activity solely in hepatocytes or cardiomyocytes, while Cas9 was efficiently inhibited in off-target cells. We demonstrate control of genome editing and gene activation using a miR-dependent AcrIIA4 in combination with different *Streptococcus pyogenes (Spy)*Cas9 variants (full-length Cas9, split-Cas9, dCas9-VP64). Finally, to showcase its modularity, we adapted our Cas-ON system to the smaller and more target-specific *Neisseria meningitidis (Nme)*Cas9 orthologue and its cognate inhibitors AcrIIC1 and AcrIIC3. Our Cas-ON switch should facilitate cell-specific activity of any CRISPR–Cas orthologue, for which a potent anti-CRISPR protein is known.

INTRODUCTION

CRISPR (clustered regularly-interspaced short palindromic repeats) technologies provide an efficient and simple means to perform targeted genetic manipulations in living cells and animals (1–5). Today, the rapidly expanding CRISPR toolbox enables genomic knock-ins/-outs (2,3), gene silencing and activation (6–8), epigenetic reprogramming (9–11), as well as single-base editing (12,13). These tools facilitate detailed genetic studies in cells and animals and hold enormous potential for the future treatment of genetic disorders (14).

With respect to *in vivo* application of CRISPR technologies, strategies to confine CRISPR–Cas9 activity to selected cells and tissues are highly desired. For genetic studies in animals, for instance, confining perturbations to selected cells is critical when aiming at disentangling the role of selected cell types in a particular phenotype or simply to avoid negative side-effects and/or artefacts that would arise from unspecific perturbations. Moreover, in the context of therapeutic genome editing within human patients, ensuring maximum specificity and hence safety of a treatment is absolutely critical. Until today, however, virtually any mode of efficient *in vivo* delivery of the CRISPR–Cas components (e.g. via viral vectors, nanoparticles, lipophilic complexes etc.) is likely to affect many cell types and tissues beyond the one of ac-

*To whom correspondence should be addressed. Tel: +49 6221 54 51287; Fax: +49 6221 54 51488; Email: dominik.niopek@bioquant.uni-heidelberg.de
Correspondence may also be addressed to Dirk Grimm. Tel: +49 6221 54 51339; Fax: +49 6221 54 51481; Email: dirk.grimm@bioquant.uni-heidelberg.de
Correspondence may also be addressed to Roland Eils. Tel: +49 30 450 54 3084; Fax: +49 30 450 7576902; Email: roland.eils@bihealth.de

tual (therapeutic) interest. This limited specificity, in turn, causes substantial risks of (treatment) side-effects (14,15).

One strategy to address this limitation would be to render the activity of the CRISPR components dependent on endogenous, cell-specific signals, so that the genetic perturbation is induced solely in the target cell population, but not in off-target cells. One such signal are mi(cro)RNAs, i.e. small, regulatory and non-coding RNAs that are involved in eukaryotic gene expression control (16,17). Being part of the RNA-induced silencing complex (RISC), miRNAs recognize sequence motifs present on m(essenger)RNAs that are complementary to the miRNA sequence. The RISC then typically mediates mRNA degradation, or translation inhibition or both, thereby causing a gene expression knockdown (16,17).

More than 1000 miRNAs have been described in humans (http://www.mirbase.org), and many miRNAs or miRNA combinations have been identified, which occur exclusively in selected cell types or disease states (18–23). These include, for instance, miR-122, which is selectively expressed in hepatocytes (18), or miR-1, which is highly abundant in myocytes (22,23). Such unique signatures have in the past been successfully harnessed for cell-specific expression of transgenes in cultured cells and mice (24,25). Adapting this strategy to CRISPR–Cas would thus offer an effective means to confine CRISPR-mediated perturbations to selected cell types.

We have previously shown that integrating miRNA-122 binding sites into the 3′UTR (3′ untranslated region) of a CRISPR–Cas9 transgene can be used to de-target Cas9 expression from hepatocytes (26). A subsequent study by Hirohide Saito's group expanded this approach to further miRNA candidates (miR-21 and miR-302a) (27). Moreover, they added a negative feedback loop to the system, thereby establishing a positive relation between miRNA abundance and Cas9 activity (27). To this end, the authors expressed Cas9 from an mRNA harbouring an L7Ae binding motif (K-turn), while co-expressing the L7Ae repressor from an mRNA carrying miRNA binding sites in its 5′UTR (27). The resulting Cas-ON switch enabled miRNA-dependent Cas9 activity. The system was leaky, however, and showed a <2-fold dynamic range of regulation, thereby limiting its utility for *in vivo* applications (see Discussion for details).

Here, we created a novel, robust and highly flexible cell type-specific Cas9-ON switch based on anti-CRISPR proteins (28–32) expressed from miRNA-dependent vectors. We placed AcrIIA4, a recently discovered *Streptococcus pyogenes (Spy)* Cas9 inhibitor, under miR-122 and miR-1 control, thereby confining *Spy*Cas9 activity to hepatocytes or cardiomyocytes. We first show that our system is compatible with different *Spy*Cas9 variants (full-length Cas9, split-Cas9, dCas9-VP64) and enables miRNA-dependent gene editing and gene activation with an up to ∼100-fold dynamic range of regulation. Finally, to demonstrate its modularity, we expanded our Cas-ON approach to the smaller and more target-specific *Neisseria meningitidis* (*Nme*)Cas9 and its cognate inhibitors AcrIIC1 and AcrIIC3.

MATERIALS AND METHODS

Cloning

A list of all constructs used and created in this study is shown in Supplementary Table S1. Annotated vector sequences are provided as Supplementary Data (GenBank files). Plasmids were created using classical restriction enzyme cloning, Golden Gate Assembly (33) or Gibson assembly (New England Biolabs). Oligonucleotides were obtained from Integrated DNA Technologies (IDT) or Sigma-Aldrich. Synthetic, double-stranded DNA fragments (gBlocks) were obtained from IDT.

Luciferase knockdown reporters carrying miRNA binding sites within the 3′UTR of the *Renilla* luciferase gene (psiCheck-2 2xmiR-122, 2xmiR-1 or 2x scrambled target sites) were generated by inserting a DNA fragment encoding two miRNA target sites followed by a bovine growth hormone (BGH) polyA signal into the psiCheck2 vector (Promega) via XhoI/NotI. The CMV promoter-driven *Spy*Cas9 expression vector (Addgene plasmid #113033) was previously developed by us (34). A *Spy*Cas9-GFP fusion was cloned by PCR-amplifying EGFP from vector pSpCas9(BB)-2A-GFP (Addgene plasmid #48138, which was a kind gift from Feng Zhang) followed by insertion of the PCR amplicon into the *Spy*Cas9 vector via EcoRI/HindIII. The AcrIIA4 and mCherry-AcrIIA4 coding sequences were obtained as human codon-optimized, synthetic DNA fragments from IDT and cloned into pcDNA3.1$^{(-)}$ (ThermoFisher) via NheI/NotI. 2xmiR-122 target sites, 2xmiR-1 target sites or a scaffold sequence identical in length but lacking the miR target sites were inserted into the resulting vectors by oligo cloning via EcoRI/HindIII, yielding vectors CMV-(mCherry)-AcrIIA4–2x*miR-122*, CMV-AcrIIA4-2x*miR-1* and CMV-(mCherry)-AcrIIA4–*scaffold*.

The luciferase cleavage reporter for measuring *Spy*Cas9 activity was previously reported by us (34). It comprises an SV40 promoter-driven *Renilla* luciferase gene, a TK promotor-driven Firefly luciferase gene, and an H1 promoter-driven sgRNA targeting the Firefly luciferase gene. The pRL-TK vector encoding *Renilla* luciferase was obtained from Promega. AAV vectors encoding (i) *Spy*Cas9 (Addgene #113034) or (ii) an H1 or U6 promoter-driven sgRNA (F+E scaffold (35)) and a RSV promoter-driven EGFP (Addgene #113039) were previously reported by us (36). Annealed oligonucleotides corresponding to the genomic target site were cloned into the sgRNA AAV vector via BbsI using Golden Gate cloning (33). All sgRNA target sites relevant to this study are shown in Supplementary Table S2. AAV vectors encoding CMV or EF1α promoter-driven AcrIIA4 variants were created by replacing the RSV promoter-driven GFP expression cassette from the sgRNA plasmids (36) with synthetic DNA fragments encoding CMV-FLAG-AcrIIA4-*scaffold*, CMV-FLAG-AcrIIA4-*2xmiR-122*, CMV-FLAG-AcrIIA4-*2xmiR-1*, EF1α-AcrIIA4-*scaffold* or EF1α-AcrIIA4-*2xmiR-122,* all succeeded by a BGH terminator sequence. AAV vectors encoding a CMV promoter-driven mCherry-AcrIIA4-*scaffold* or mCherry-AcrIIA4-2x*miR-122* were obtained by

replacing the ITR-flanked transgene cassette in the sgRNA plasmids (36) with respective PCR fragments based on the mCherry-AcrIIA4 vectors described above. A vector for AAV-mediated expression of YFP (scAAV-YFP) was previously reported by us (37).

An AAV vector co-encoding an N-terminal *Spy*Cas9 fragment fused to a split-intein and a U6 promoter-driven sgRNA scaffold (F+E) was generated by inserting a DNA fragment encoding the U6-promoter-sgRNA scaffold via MluI/XbaI into vector pAAV-SMVP-Cas9N (kind gift from George Church (Addgene plasmid #80930)). An AAV vector co-encoding the corresponding C-terminal *Spy*Cas9 fragment fused to a split-intein was a kind gift from George Church (Addgene plasmid #80931). CMV promoter-driven AcrIIA4 fragments with or without 2xmiR-122 target sites were introduced into this vector by first inserting unique XbaI and MluI sites behind the SV40 polyA. These were subsequently used to introduce CMV-AcrIIA4-*scaffold* and CMV-AcrIIA4-*2xmiR-122* fragments generated by PCR from corresponding template vectors described above.

The pAAV-pSi vector co-encoding Firefly and *Renilla* luciferase (pAAV-pSi) was previously reported by us (36). A single miR-1 binding site was introduced into the *Renilla* luciferase gene 3′UTR by oligo cloning via XhoI/NotI resulting in the vector pAAV-pSi 1xmiR target site.

The CMV-miR-122 expression construct was previously reported by us (38). The CMV-miR-1 expression vector was created by replacing the miR-122 coding sequence in vector CMV-miR-122 by the miR-1 coding sequence, which we obtained via restriction digest of pTRE_Tight_miR-1 (kind gift from David Bartel, Addgene plasmid #14896) with BamHI/HindIII. The Tet-inducible luciferase reporter and corresponding sgRNA construct (sgRNA1_Tet-inducible Luciferase reporter) were kind gifts from Moritoshi Sato (Addgene plasmids #64127 and #64161). dCas9-VP64_GFP was a kind gift from Feng Zhang (Addgene plasmid #61422). The pEJS654 All-in-One AAV-sgRNA-hNmeCas9 vector was a kind gift from Erik Sontheimer (Addgene plasmid #112139). The VEGFA target site (NTS-33 (Ref. 39)) was introduced into this vector by oligo cloning via SapI. The AcrIIC1 and AcrIIC3 coding sequences were obtained as human codon-optimized, synthetic DNA fragment from IDT and cloned into the AAV CMV promoter-driven AcrIIA4-*scaffold or* AAV CMV promoter-driven AcrIIA4-*2xmiR-122* vectors by replacing the AcrIIA4 sequences with the AcrIIC1 or AcrIIC3 coding sequences.

In all cloning procedures, PCRs were performed using Phusion Flash High-Fidelity polymerase (ThermoFisher) or Q5 Hot Start High-Fidelity DNA Polymerase (New England Biolabs) followed by agarose gel electrophoresis to analyse PCR products. Bands of the expected size were cut out and the DNA was extracted by using a QIAquick Gel Extraction Kit (Qiagen). Restriction digests and ligations were performed with enzymes from New England Biolabs and ThermoFisher and according to the manufacturer's protocols. Chemically-competent Top10 cells (ThermoFisher) were used for plasmid amplification and plasmid DNA was purified using the QIAamp DNA Mini, Plasmid Plus Midi or Plasmid Maxi Kit (all from Qiagen).

Cell culture

Cells lines were cultured at 5% CO_2 and 37°C in a humidified incubator and passaged when reaching 70–90% confluency. HeLa and HEK293T cells were maintained in 1× DMEM without phenol red (ThermoFisher) supplemented with 10% (v/v) fetal calf serum (Biochrom AG), 2 mM L-glutamine and 100 U per mL penicillin/100 μg per mL streptomycin (both ThermoFisher). Huh-7 medium was additionally supplemented with 1 mM non-essential amino acids (ThermoFisher). HeLa, HEK293T and Huh-7 cells were authenticated and tested for mycoplasma contamination prior to use via a commercial service (Multiplexion). HL-1 cells were cultured in Claycomb medium supplemented with 10% (v/v) fetal calf serum, 1% penicillin/streptomycin, 0.1 mM norepinephrine, and 2 mM L-glutamine on plates pre-coated with 0.02% (w/v) gelatin and 5 μg/ml fibronectin (all Sigma-Aldrich).

Cells were transfected with Lipofectamine™2000, Lipofectamine™3000 (both ThermoFisher) or jetPRIME® (Polyplus-transfection) according to the manufacturers' protocols and as specified in the experimental sections below.

Fluorescence microscopy

For the AcrIIA4 knockdown experiment in Figure 1C, HeLa and Huh-7 cells were seeded into 8-well Glass Bottom μ-Slides (ibidi) at a density of 30 000 cells per well for HeLa cells and of 60 000 cells per well for Huh-7 cells in 300 μl media. The next day, cells were transfected using 1.85 μl Lipofectamine™2000 per well by following the manufacturer's protocol. The total amount of transfected DNA per well was 720 ng evenly split between plasmids encoding *Spy*Cas9-GFP, either mCherry-AcrIIA4-*scaffold* or AcrIIA4-*2xmiR-122*, and the luciferase cleavage reporter plasmid (to provide a sgRNA and an exogenous target). The medium was exchanged 6 h post-transfection.

Twenty-four hours post-transfection, HeLa and Huh-7 cells were treated with Hoechst 33342 solution at a final concentration of 5 μg per mL for 15 min at 37°C. Then, the medium was replaced and imaging was performed using a Leica SP8 confocal laser scanning microscope equipped with automated CO_2 and temperature control, a UV, argon, and a solid state laser, as well as a HCX PL APO 20× oil objective (N/A = 0.7). mCherry fluorescence was recorded using the 552 nm laser line for excitation and the detection wavelength was set to 578–789 nm. GFP fluorescence was recorded using the 488 nm laser line for excitation and the detection wavelength was set to 493–578 nm.

To investigate the transduction efficiency of AAV2 (Supplementary Figure S5), HeLa, Huh-7 and HEK293T cells were seeded into 96-well plates at a density of 4000 cells and using a volume of 100 μl media per well. Each well contained 10 μl of AAV2 lysate encoding a YFP reporter, i.e. cells were transduced while seeding (reverse transduction). Seventy-two hours post-transduction, cells were fixed with 4% PFA for 30 min and subsequently stained with Hoechst 33342 (ThermoFisher). Images were acquired with a 10× objective in nine positions per well with a fully automated epifluorescence Scan∧R screening microscope. To

obtain quantitative values for transduction efficiencies (percentages of YFP-positive cells) and for mean expression intensities per cell, a previously established microscopy-based assay for quantitative analysis was used (40).

Western blot

For Western blot analysis (Figure 1D), cells were seeded into 6-well plates (CytoOne) at a density of 300 000 cells per well for HeLa cells and 450 000 cells per well for Huh-7 cells. The following day, cells were co-transfected with 500 ng of *Spy*Cas9-GFP and either 500 ng CMV-mCherry-AcrIIA4-*scaffold* or CMV-mCherry-AcrIIA4-*2xmiR-122* per well using Lipofectamine™3000. Twenty-four hours post-transfection, the media was aspirated from the culture plates and the cells were washed with ice-cold PBS. Fifty microliters of protein lysis buffer (150 mM NaCl, 10 mM Tris, 1 mM EDTA, 0.5% NP-40 and 10% cOmplete Protease Inhibitor (Roche), pH 8.0) were added, and the cells were detached from the culture plate surface using a cell scraper. The cell suspension was then transferred into a 1.5 ml tube, incubated for 20 min on ice, and centrifuged for 10 min at 13 200 rpm (15 974 × g) and 4°C. The supernatant containing the protein lysate was transferred into a new 1.5 ml tube and protein concentrations were measured using the Bradford Reagent (Sigma-Aldrich) according to the manufacturer's protocol. Fifty microgram of protein lysate were then mixed with 4× Laemmli Sample Buffer (Bio-Rad), and the volume of each sample was adjusted to 30 μl using lysis buffer. The samples were denatured for 10 min at 95°C, cooled down on ice and loaded on a 10% Bis–Tris gel (Life Technologies). Proteins were then separated by molecular weight by applying 130 V for 120 min in 1× MOPS buffer (Life Technologies). Next, proteins were transferred onto a nitrocellulose membrane (pore size: 0.2 μm) (Millipore) by using 1× borate transfer buffer (20 mM boric acid, 1 mM EDTA, 6.25 mM NaOH) and applying 300 mA current overnight. The membrane was then cut at ∼72 and ∼45 kDa, and washed in TBS-T (Tris-buffered saline (20 mM Tris, 140 mM NaCl, pH7.6) supplemented with 0.1% Tween 20 (Sigma-Aldrich)) and blocked by incubation in 5% milk (skim milk powder, GERBU Biotechnik GmbH, diluted in TBS-T) at room temperature for 1 h. GFP antibody (ChromoTek, diluted 1:1500) was used for *Spy*Cas9-GFP detection (190 kDa), α-tubulin antibody (Santa Cruz Biotechnology, diluted 1:500) was used for α-tubulin detection (55 kDa) and RFP antibody (ChromoTek, diluted 1:500) was used for mCherry-AcrIIA4 detection (38 kDa). All antibodies were diluted in 5% milk in TBS-T, added to the corresponding membrane piece and incubated overnight at 4°C while shaking. The next day, the membrane was washed three times for 5 min in TBS-T followed by incubation with HRP-(horse radish peroxidase-)linked secondary antibodies (anti-mouse antibody, 1:5000 in 5% milk in TBS-T (Dianova) or anti-rat antibody, 1:1000 in 5% milk in TBS-T (Jackson ImmunoResearch)) for 1 h at room temperature. The membrane was then washed three times for 5 min in TBS-T to remove unbound antibodies and SuperSignal™ West Pico PLUS Chemiluminescent Substrate (ThermoFisher) was applied for 5 min. Finally, the luminescence signal was detected using a ChemoStar detector (INTAS). The full-length Western blot image is shown in Supplementary Figure S1.

Luciferase assays

For luciferase experiments, HeLa and Huh-7 cells were seeded at a density of 6000 cells per well, HEK293T cells were seeded at a density of 12 500 cells per well, and HL-1 cells were seeded at a density of 12 000 cells per well into 96-well plates (Eppendorf) using 100 μl culture medium per well. Sixteen hours post-seeding, cells were either transiently transfected or transduced with AAV vectors as specified below (all plasmid/vector amounts are per well).

For miR-122- or miR-1-induced *Renilla* luciferase knockdown experiments (Supplementary Figures S3 and S9), Huh-7, HeLa and HEK293T cells were transfected with 20 ng of psiCheck-2 reporter (with or without 2xmiR-122 target sites within the *Renilla* luciferase 3′UTR) and 80 ng of an irrelevant stuffer DNA (pcDNA3.1$^{(-)}$, ThermoFisher). HL-1 cells were pre-treated with 0.5 μM of Bortezomib (Biomol) to improve transduction efficiency and then transduced with 10 μl pAAV-pSi vector per well (with or without miR-1 binding site within the *Renilla* 3′UTR; see below for AAV production).

For *Spy*Cas9 luciferase cleavage experiments (Figure 2A and Supplementary Figure S4), cells were co-transfected with 20 ng luciferase cleavage reporter plasmid, 20 ng CMV-*Spy*Cas9 expression vector, and different doses of AcrIIA4-*scaffold* or AcrIIA4-*2xmiR-122* expression vectors (0.25, 1, 5 or 20 ng, indicated in the figure legends). For split-*Spy*Cas9 luciferase cleavage experiments (Supplementary Figure S8), cells were co-transfected with 20 ng luciferase cleavage reporter plasmid, 20 ng of AAV N-*Spy*Cas9-Intein and 20 ng of either (i) AAV Intein-C-*Spy*Cas9, (ii) AAV Intein-C-*Spy*Cas9-CMV-AcrIIA4-*scaffold* or (iii) AAV Intein-C-*Spy*Cas9-CMV-AcrIIA4-*2xmiR-122*. To keep the total amount of DNA transfected constant between all samples, DNA was topped up to 100 ng per well using an irrelevant stuffer DNA (pcDNA3.1$^{(-)}$).

For miR-122- or miR-1-induced *Renilla* luciferase knockdown experiments (Supplementary Figure S11A), HEK293T cells were co-transfected with 20 ng psiCheck-2 reporter (with 2xmiR-122 target sites, 2xmiR-1 target sites or 2x scrambled target sites within the *Renilla* luciferase 3′UTR) and 80 ng of either miR-122 or miR-1 expression plasmid, or an irrelevant stuffer DNA (pcDNA3.1$^{(-)}$). For *Spy*Cas9 luciferase cleavage experiments (Supplementary Figure S11B), cells were co-transfected with (i) 20 ng luciferase cleavage reporter plasmid, (ii) 20 ng CMV-*Spy*Cas9 expression vector, (iii) 20 ng of AcrIIA4-*scaffold,* AcrIIA4-*2xmiR-122* or AcrIIA4-*2xmiR-1* expression vectors and (iv) 80 ng of either miR-122 or miR-1 expression plasmid, or an irrelevant stuffer DNA.

For *Spy*dCas9-VP64-mediated luciferase activation experiments (Figure 3B), cells were co-transfected with 20 ng Tet-inducible luciferase reporter plasmid, 20 ng dCAS9-VP64_GFP expression vector, 20 ng sgRNA1_Tet-inducible luciferase reporter, 1 ng pRL-TK (encoding *Renilla* luciferase, Promega), and different doses (1, 5, 10, 20, 40 or 60 ng, indicated in the corresponding figure legends) AcrIIA4

expression vector. DNA was topped up to 101 ng per well using an irrelevant stuffer DNA (pcDNA3.1(–)).

Six hours post-transfection or 4 h post-transduction, the medium was replaced. HeLa, Huh-7 and HEK293T cells were incubated for 48 h and HL-1 cells were incubated for 72 h before measuring *Renilla* and Firefly luciferase activity using a Dual-Glo Luciferase Assay System (Promega) according to the manufacturer's recommendation. In brief, cells were harvested in the supplied lysis buffer and Firefly and *Renilla* luciferase activities were measured using a GLOMAX™ Discover or GLOMAX™ 96-microplate luminometer (both Promega). Integration time was 10 s, and delay time between automated substrate injection and measurement was 2 s. For the miRNA-dependent luciferase knockdown experiments based on the psiCheck-2 and pAAV-pSi vectors, *Renilla* luciferase photon counts were normalized to the Firefly luciferase photon counts (as miR target sites were inserted into the *Renilla* luciferase 3′UTR). For *Spy*Cas9 luciferase cleavage experiments and *Spy*dCas9-VP64-mediated luciferase activation experiments, Firefly luciferase photon counts were normalized to *Renilla* photon counts (as Cas9 is targeting the Firefly luciferase gene in these assays).

AAV lysate production

For production of AAV-containing cell lysates, low-passage HEK293T cells were seeded into 6-well plates (CytoOne) at a density of 350 000 cells per well. The following day, cells were triple-transfected with (i) the AAV vector plasmid, (ii) an AAV helper plasmid carrying AAV serotype 2 (AAV2) *rep* and either the AAV2 (when targeting Huh-7, HeLa or HEK293T cells) or AAV6 *cap* genes (when targeting HL-1 cells) and (iii) an adenoviral plasmid providing helper functions for AAV production, using 1.33 μg of each construct and 8 μl of TurboFect Transfection Reagent (ThermoFisher) per well. The AAV vector plasmid encoded either (i) *Spy*Cas9 driven from an engineered, short CMV promoter, (ii) a U6 promoter-driven sgRNA (based on the improved F+E *Spy*Cas9 scaffold), and a RSV promoter-driven GFP marker, (iii) a CMV promoter-driven AcrIIA4, AcrIIC1 or AcrIIC3 either with or without two miRNA binding sites in their 3′UTRs, (iv) U1a promoter-driven *Nme*Cas9 co-encoding a U6 promoter-driven sgRNA (VEGFA or non-targeting control), or (v) a CMV promoter-driven YFP. Seventy-two hours post-transfection, cells were collected in 300 μl PBS and subsequently subjected to five freeze-thaw cycles by alternating between snap freezing in liquid nitrogen and a 37°C water bath. The cell debris was removed by centrifugation at ∼18 000 × g for 10 min and the AAV-containing supernatant was stored at −20°C until use.

T7 assays and TIDE sequencing

For transduction-based T7 assays, HeLa and Huh-7 cells were seeded at a density of 3000 cells per well, HEK293T cells were seeded at a density of 3500 cells per well, and HL-1 cells were seeded at a density of 12 000 cells per well into 96-well plates (Eppendorf) using 100 μl culture medium per well. Sixteen hours post-seeding, cells were co-transduced with AAV lysates encoding Cas9, a sgRNA, and the respective anti-CRISPR variant. For experiments targeting the EMX1, CCR5 or AAVS1 locus Figure 2B–D), Huh-7 and HeLa cells were transduced with 33 μl of *Spy*Cas9 vector lysate, 33 μl of EMX1, CCR5 or AAVS1 sgRNA vector lysate, and either 1, 2.5, 5, 7.5 or 10 μl of either AcrIIA4-*scaffold* or AcrIIA4-*2xmiR-122* vector lysate (as indicated in the figure legends). For experiments targeting the VEGFA locus (Figure 4), Huh-7 and HEK293T cells were transduced with 40 μl of the *Nme*Cas9 AAV lysate and either 5, 10 or 20 μl of AcrIIC1 AAV lysate or 2.5, 5 or 10 μl of AcrIIC3 AAV lysate (as indicated in the figure legends). HL-1 cells were co-transduced with AAV lysates comprising 10 μl of the *Spy*Cas9 vector, 10 μl of the Rosa-26 sgRNA vector, and 3 μl of either AcrIIA4-*scaffold* or AcrIIA4-*2xmiR-1* vector (Figure 2G and Supplementary Figure S10).

The volume of the AAV lysate used per well was adjusted with PBS to 100 μl for *Spy*Cas9 experiments in HeLa and Huh-7 cells, to 80 μl for *Nme*Cas9 experiments in Huh-7 and HEK293T cells, and to 23 μl for T7 assays in HL-1 cells, so that the total volume per well was identical in all samples, including the positive (Cas9 plus sgRNA, but no Acr) and negative (Cas9 only) controls. Medium was replaced 24 h (for HEK293T, HeLa and Huh-7 cells) or 4 h (for HL-1) post-infection and the transduction was repeated 24 h after the first transduction started.

For transfection-based T7 assays (Supplementary Figure S11C and D), HEK293T cells were seeded at a density of 12 500 cells per well into 96-well plates (Eppendorf) using 100 μl culture medium per well. Sixteen hours post-seeding, cells were co-transfected with (i) 25 ng of *Spy*Cas9, (ii) 25 ng of sgRNA construct targeting either the EMX1 or CCR5 locus, (iii) 25 ng of AcrIIA4-*scaffold,* AcrIIA4-*2xmiR-122* or AcrIIA4-*2xmiR-1* and (iv) 125 ng of either miR-122 or miR-1 expression plasmid, or empty vector using jetPRIME® (Polyplus-transfection) according to the manufacturers' protocol.

Seventy-two hours after the (first) transduction or transfection, cells were lysed using DirectPCR lysis reagent supplemented with proteinase K (Sigma-Aldrich). The genomic target locus was PCR-amplified with primers flanking the target site (Supplementary Table S3) using Q5 Hot Start High-Fidelity DNA Polymerase (New England Biolabs). For TIDE sequencing analysis (Figure 2F and Supplementary Figures S6 and S12), the amplicon was purified using gel electrophoresis followed by gel extraction using the QIAquick Gel Extraction Kit (Qiagen) and by Sanger sequencing (Eurofins). Data analysis was performed using the TIDE web tool (https://tide.deskgen.com/) (41). To assess the indel frequency by T7 assay, we employed a rapid T7 protocol (26). Ten microliters of the target locus amplicons were diluted 1:4 in 1× buffer 2 (New England Biolabs), heated up to 95°C, and slowly cooled down to allow re-annealing and formation of hetero-duplexes using a nexus GSX1 Mastercycler (Eppendorf) and the following program: 95°C/5 min, 95–85°C at −2°C/s, 85–25°C at −0.1°C/s. Subsequently, 0.5 μl T7 endonuclease (New Eng-

land Biolabs) was added, samples were mixed and incubated at 37°C for 15 min followed by analysis on a 2% Tris–borate–EDTA agarose gel. The Gel iX20 system equipped with a 2.8 megapixel/14 bit scientific-grade CCD camera (INTAS) was used for gel documentation. To calculate the indel percentages from the gel images, the background was subtracted from each lane and T7 bands were quantified using the ImageJ (http://imagej.nih.gov/ij/) gel analysis tool. Peak areas were measured and percentages of insertions and deletions (indel(%)) were calculated using the formula indel (%) = $100 \times (1 - (1 - \text{fraction cleaved})^{1/2})$, whereas the fraction cleaved = $\sum$(cleavage product bands)/$\sum$(cleavage product bands + PCR input band). Full-length T7 assay gel images are shown in Supplementary Figure S2.

Flow cytometry

For flow cytometry experiments (Supplementary Figure S7), Huh-7 cells were seeded at a density of 18 000 cells per well into 24-well plates (greiner bio-one) using 1 ml culture medium per well. Sixteen hours post-seeding, cells were transduced with 6, 30 or 60 μl AAV lysates encoding either mCherry-AcrIIA4-*scaffold* or mCherry-AcrIIA4-*2xmiR-122*. Of note, these volumes are equivalent to 1, 5 or 10 μl of AcrIIA4 AAV lysate applied in T7 assays in 96-well format (Figure 2B–D), in which a sixth of the cell number was used (3000 cells per compartment) as compared to the 24-well format (18 000 cells per compartment). The volume of the AAV lysate used per well was adjusted to 100 μl with PBS. Twenty-four hours post-transduction, medium was replaced and the transduction repeated. Seventy-two hours after the (first) transduction, cells were washed with PBS, detached from the cell surface by trypsinization, and collected in 200 μl PBS. Flow cytometry was performed on a FACSCanto (BD Biosciences) system equipped with 405, 488 and 561 nm lasers. Per condition, 8000–10 000 events were recorded. Data analysis was performed using the FACSDiva 8.0 (BD Biosciences) software package, applying the gating strategy shown in Supplementary Figure S7A.

Statistical analysis

Independent experiments correspond to cell samples seeded, transfected and treated independently and on different days. Uncertainties in the reported mean values are indicated as the standard error of the mean (s.e.m.). A two-sided Student's *t*-test was applied to test differences in reported mean values for statistical significance. *P*-values were Bonferroni corrected to account for the multiple, pairwise comparisons made. Made comparisons (as indicated by the brackets in the figures) thereby always correspond to identical doses of Acr construct with and without miRNA binding sites present in their 3′UTR. We made these particular comparisons, as they enable assessing the miRNA-dependent regulation of Cas9 activity for statistical significance. Resulting *P*-values < 0.05, 0.01 and 0.001 are indicated by one, two or three asterisks, respectively. Table 1 shows *P*-values, significance levels (asterisks), and corresponding effect sizes (fold changes) for all made comparisons.

RESULTS

Design of miRNA-dependent anti-CRISPR vectors

To generate a cell-specific Cas9-ON switch, we aimed at rendering the activity of CRISPR–Cas9 dependent on the presence of cell-specific miRNAs, i.e. miRNAs that are abundant solely within the target cell type. Translating the abundance of a miRNA, which typically is a negative stimulus (causing gene expression knockdown), into a positive output (Cas9 activity) requires a negative feedback.

We hypothesized that anti-CRISPR proteins, a recently discovered class of phage-derived CRISPR–Cas inhibitors (28,30,42,43), would be an ideal mediator to establish this negative feedback. Due to their small size (∼80–150 amino acids), Acrs can be expressed quickly and efficiently from plasmids or viral vectors. More importantly, anti-CRISPR proteins block CRISPR–Cas9 DNA targeting, Cas9 nuclease function or both by directly binding to the Cas9/sgRNA complex. This post-translational inhibitory mechanism enables a complete shutdown of CRISPR–Cas9 activity even upon simultaneous delivery of Cas9, a sgRNA, and an anti-CRISPR-encoding vector (29–31,44). We hypothesized that coupling the expression of anti-CRISPR proteins to cell-specific miRNAs by integrating miRNA target sites into the 3′UTR of *acr* transgenes should result in a cell type-specific Cas9-ON switch (Figure 1A). In on-target cells expressing the respective miRNA at high levels, Acr expression would be efficiently knocked down, thereby permitting CRISPR–Cas9 activity. In off-target cells lacking the respective miRNA, however, the Acr would remain expressed at high levels, thereby blocking Cas9 function selectively in these cells.

To validate this concept, we created a modular vector encoding a CMV promoter-driven AcrIIA4, a potent inhibitor of the most widely employed Cas9 orthologue from *S. pyogenes* (30). BsmBI (Esp3I) sites present in the 3′UTR of the AcrIIA4 gene enable the introduction of miRNA target sites via Golden Gate cloning, so that AcrIIA4 expression can be set under control of any abundant, cell-specific miRNA (or set of miRNAs, see Discussion).

A prominent example is miR-122, which is highly expressed in the liver, but not in any other tissue (18). Using a luciferase reporter knockdown assay, we could confirm a strong miR-122 expression in human hepatocellular carcinoma cells (Huh-7), while human cervix carcinoma (HeLa) or embryonic kidney (HEK293T) control cells showed comparably low miR-122 levels (Supplementary Figure S3).

To place AcrIIA4 under miR-122 regulation, we inserted a concatemer of two miR-122 target sites into our modular AcrIIA4 construct. We further added an N-terminal mCherry to enable fluorescence-based detection of AcrIIA4 expression (Figure 1B). Then, we co-transfected the resulting vector (mCherry-AcrIIA4-*2xmiR-122*) or a control vector (mCherry-AcrIIA4-*scaffold*) alongside a *Spy*Cas9-GFP vector into Huh-7 and HeLa cells. The control vector contained two scrambled miRNA binding sites for which no complementary miRNA is known. Live-cell fluorescence microscopy and complementary Western blot analysis revealed an efficient knockdown of mCherry-AcrIIA4-*2xmiR-122* expression in Huh-7, but not in HeLa cells,

Table 1. Summary of statistical analysis

Figure	Cell line	Dose/miRNA	*P*-value	Significance level	Fold change
Figure 2A	Huh-7	20ng	0.0004	***	3.2
		5ng	< 0.0001	***	8.5
	HeLa	20ng	1.7242	n.s.	1.0
		5ng	0.4322	n.s.	1.2
Figure 2B	Huh-7	5μl	0.0075	**	10.5
		7.5μl	< 0.0001	***	11.4
		10μl	0.0018	**	16.1
	HeLa	5μl	0.8160	n.s.	1.3
		7.5μl	2.5254	n.s.	0.8
		10μl	2.4297	n.s.	1.3
Figure 2C	Huh-7	1μl	0.0081	**	2.6
		2.5μl	0.0015	**	6.7
		5μl	0.0369	*	14.3
Figure 2D	Huh-7	1μl	0.1149	n.s.	1.5
		2.5μl	0.0045	**	4.5
		5μl	0.0087	**	13.0
Figure 3B	Huh-7	60ng	0.0080	**	114.0
		40ng	< 0.0001	***	54.0
		20ng	< 0.0001	***	45.4
		10ng	0.0036	**	11.4
		5ng	0.3000	n.s.	3.7
		1ng	0.7338	n.s.	1.5
Figure 4A	Huh-7	5μl	0.0072	**	2.9
		10μl	< 0.0001	***	5.7
		20μl	< 0.0001	***	24.2
	HEK293T	5μl	0.3279	n.s.	3.1
		10μl	0.2556	n.s.	5.4
		20μl	2.7279	n.s.	0.9
Figure 4B	Huh-7	2.5μl	< 0.0001	***	3.4
		5μl	0.0087	**	7.8
		10μl	0.0078	**	12.5
	HEK293T	2.5μl	2.4603	n.s.	0.9
		5μl	2.4537	n.s.	0.9
		10μl	1.9962	n.s.	1.4
Supplementary Figure S8	Huh-7	20ng	0.0018	**	4.2
	HeLa	20ng	0.8608	n.s.	1.0
Supplementary Figure S11B	HEK293T	scaffold	0.6523	n.s.	1.0
			0.2221	n.s.	0.9
		2xmiR-122	0.0015	**	3.2
			0.9901	n.s.	1.0
		2xmiR-1	0.2232	n.s.	0.8
			0.0012	**	5.4

thereby indicating a successful coupling of miRNA-122 abundance to AcrIIA4 expression (Figure 1C, D). As expected, *Spy*Cas9-GFP expression was not affected by the AcrIIA4 knockdown (Figure 1C, D).

Hepatocyte- and cardiomyocyte-specific *Spy*Cas9 activity

To investigate whether the observed, miR-122-dependent knockdown of AcrIIA4 would be sufficient to permit CRISPR–Cas9 activity specifically in hepatocytes, we performed a luciferase reporter cleavage assay. We co-transfected Huh-7 or HeLa cells with vectors encoding *Spy*Cas9, AcrIIA4-*2xmiR-122* (or AcrIIA4-*scaffold* as control) as well as a Firefly luciferase reporter plasmid, co-encoding a sgRNA targeting the Firefly luciferase gene, and measured luciferase activity 48 h post-transfection. As expected, we observed efficient reporter cleavage as indicated by the potent knockdown of Firefly luciferase activity observed specifically in the Huh-7 samples expressing AcrIIA4-*2xmiR-122*, but not in the AcrIIA4-*scaffold* control samples (Figure 2A). In contrast, *Spy*Cas9 was strongly inhibited in the HeLa control samples irrespective of the presence of miR-122 target sites in the AcrIIA4 3′UTR (Figure 2A), thereby confirming the functionality of our Cas9-ON switch. As expected, the dynamic range of miRNA-dependent Cas9 regulation in Huh-7 cells as well as Cas9 inhibition in the off-target cells (HeLa) depended on the transfected AcrIIA4 vector dose (Figure 2A) and could be further tuned by varying the strength of the AcrIIA4-driving promoter (Supplementary Figure S4).

Next, we tested whether our Cas9-ON strategy would also enable cell type-specific editing of endogenous genomic loci. To deliver the different components of our system efficiently, we chose to employ Adeno-associated virus (AAV) vectors. AAVs are highly efficient, safe (AAVs are non-pathogenic in humans), and—very importantly—can be re-targeted to specific cell types or tissues by modifying the viral capsid (45–47). These properties render AAV a prime vector candidate for therapeutic gene delivery. For delivery we chose AAV2, a well-studied AAV serotype known for its ability to transduce various cell lines (46), including Huh-7, HeLa and HEK293T (Supplementary Figure S5).

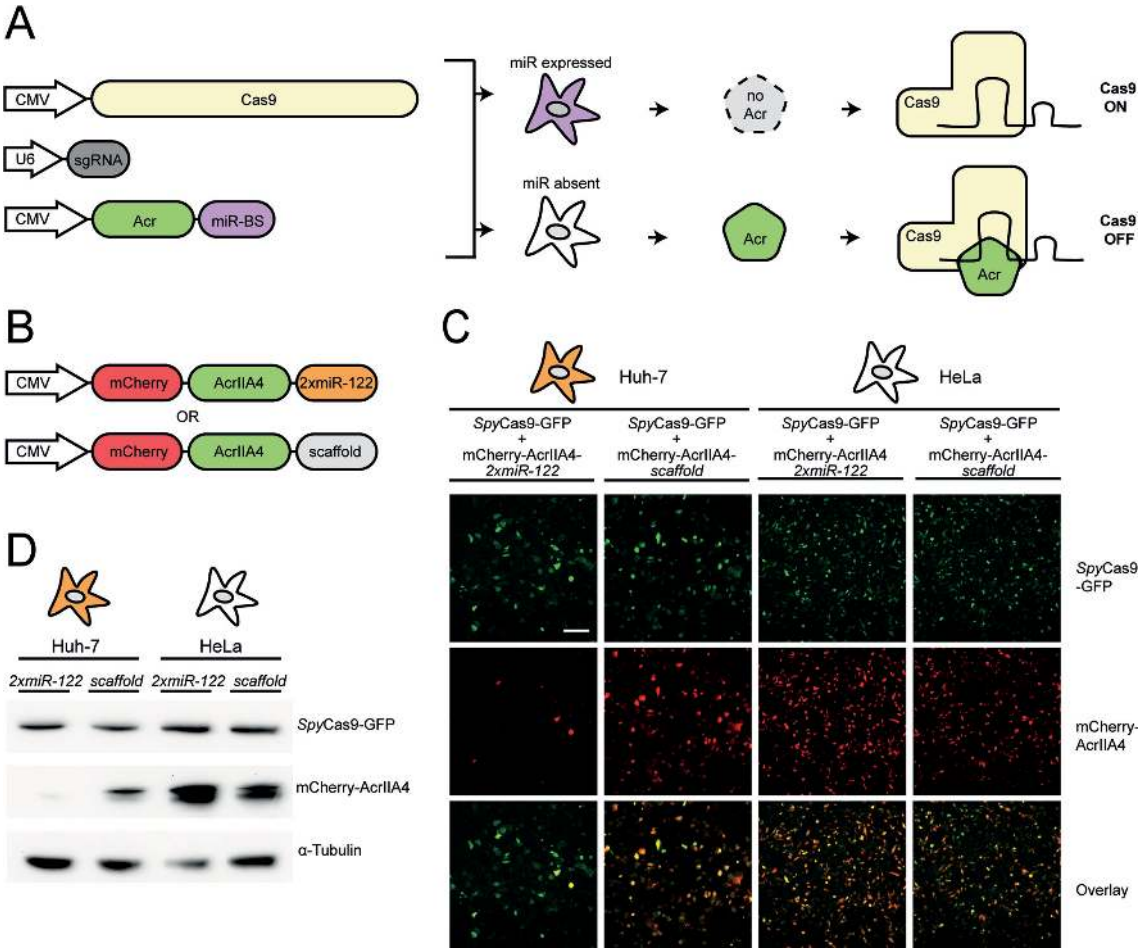

Figure 1. Designing a cell-specific Cas-ON switch based on miRNA-regulated anti-CRISPR genes. (**A**) Schematic of the Cas-ON switch. Target sites for cell-specific, abundant miRNAs are inserted into the 3′UTR of an Acr-encoding transgene. Upon delivery, a knockdown of Acr expression occurs selectively within the target cells, thereby permitting CRISPR–Cas activity. In OFF-target cells lacking the miRNA signature, the Acr protein is translated and inhibits CRISPR–Cas. (**B**) Schematics of mCherry-AcrIIA4 fusion constructs with or without 2xmiR-122 target sites. (**C, D**) Hepatocyte-specific knockdown of mCherry-AcrIIA4 expression. Huh-7 and HeLa cells co-transfected with *Spy*Cas9-GFP and either mCherry-AcrIIA4-*scaffold* or mCherry-AcrIIA4-*2xmiR-122*. (**C**) Representative fluorescence images and corresponding overlays from $n = 2$ independent experiments. Scale bar is 200 μm. (**D**) Complementary Western blot analysis of *Spy*Cas9-GFP and mCherry-AcrIIA4 expression. Data represent a single experiment.

We packaged (i) *Spy*Cas9, (ii) sgRNAs targeting the human EMX1, CCR5 or AAVS1 locus as well as (iii) AcrIIA4-*2xmiR-122* or AcrIIA4-*scaffold* into AAV2. We then co-transduced Huh-7 or HeLa cells with combinations of these vectors, while varying the AcrIIA4 vector dose, and measured the frequency of insertions and deletions at the target loci using a T7 endonuclease assay and TIDE sequencing (41). We observed potent, miRNA-122-dependent gene editing at all three target loci in Huh-7 cells with a maximum dynamic range of regulation of ∼16-fold (for EMX1, *P*-value = 0.0018; Figure 2B–D, Supplementary Figure S6). The editing efficiency in the ON state and leakiness of the system in the OFF state depended on the used AcrIIA4 vector dose (Figure 2B–D). Complementary flow cytometry analysis revealed that the system's leakiness in the OFF state at low vector doses results, at least partially, from incomplete transduction, yielding a considerable fraction of cells that do not express AcrIIA4 (Supplementary Figure S7). In contrast, while Cas9 is completely blocked in the OFF state at very high vector doses, partial inhibition of Cas9 occurred also in the system's ON state (Figure 2B–D). This is likely a result from incomplete knockdown of AcrIIA4-*2xmiR-122* at such high vector doses due to saturation of the endogenous RNAi machinery with *acr* transcripts (36) (Supplementary Figure S7). Very importantly, in HeLa control cells, Cas9 activity was equally suppressed in the presence of the AcrIIA4-*2xmiR-122* or AcrIIA4-*scaffold* vector (Figure 2B), indicating that our miRNA-122-dependent Cas9-ON switch is indeed hepatocyte-specific.

The large size of CRISPR-*Spy*Cas9 (∼1300 amino acids) poses a challenge with respect to its efficient delivery and expression, in particular when using vectors with a constrained packaging capacity. To circumvent this problem, several groups have developed split-*Spy*Cas9 variants, which comprise an N- and C-terminal Cas9 fragment that reconstitute a functional Cas9 when co-expressed within the same cell (48–51). To test whether our anti-CRISPR-based Cas9-ON strategy would also work for split-*Spy*Cas9s, we employed an intein-based split-*Spy*Cas9 system recently reported by the lab of George Church (52). We co-transfected

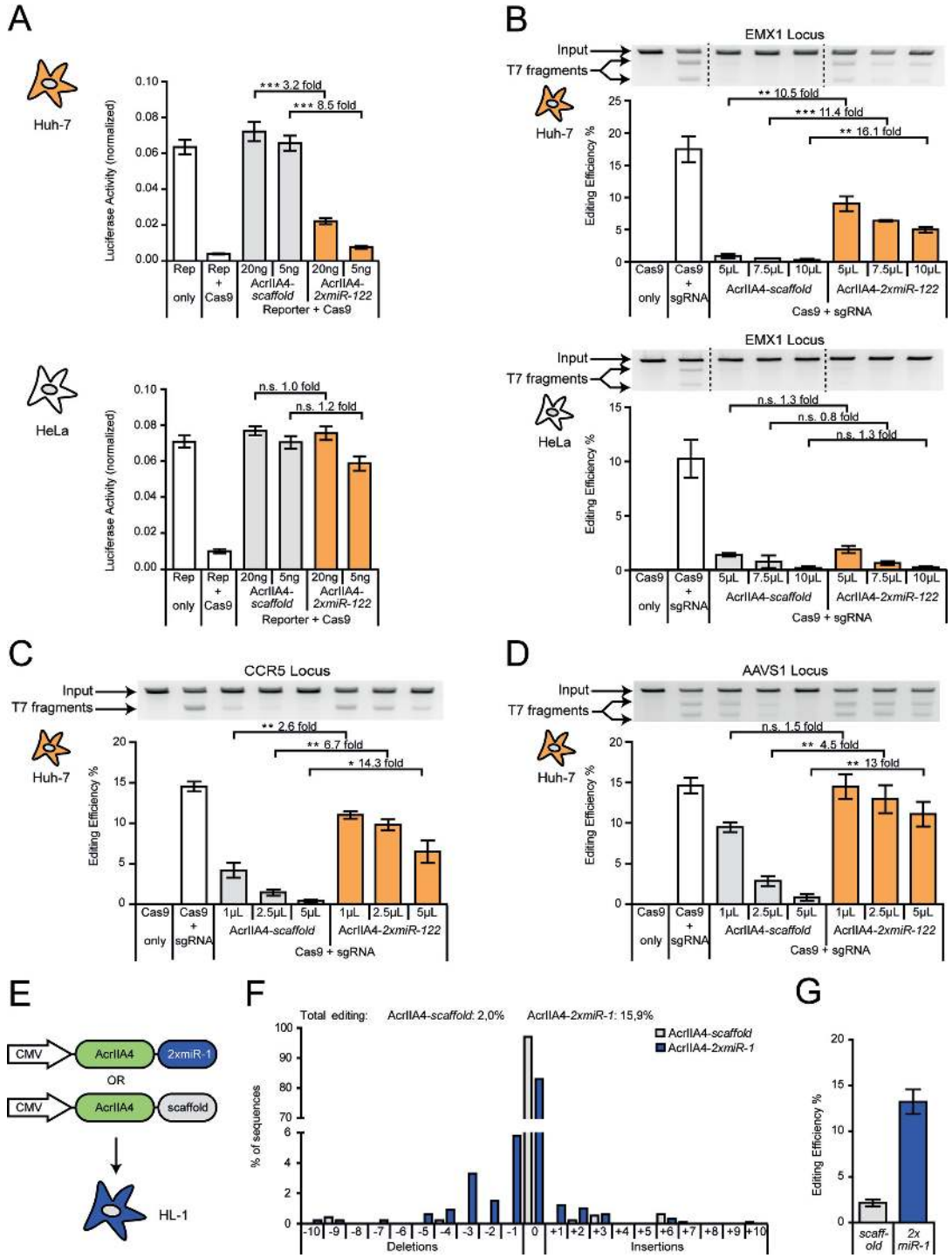

Figure 2. Hepatocyte- or cardiomyocyte-specific genome editing. (**A**) Hepatocyte-specific luciferase reporter cleavage. Huh-7 or HeLa cells were co-transfected with plasmids encoding *Spy*Cas9, a luciferase reporter, a reporter-targeting sgRNA, and AcrIIA4-*miR-122* or AcrIIA4-*scaffold*, followed by luciferase assay. During transfection, the Acr vector dose was varied as indicated. Data are means ± s.e.m. ($n = 7$ independent experiments). (**B**) Hepatocyte-specific indel mutation of the human EMX1 locus. Huh-7 and HeLa cells were co-transduced with AAV vectors encoding *Spy*Cas9, an EMX-1-targeting sgRNA, and the indicated AcrIIA4 variant, followed by T7 endonuclease assay. During transduction, the Acr vector dose was varied as indicated. Data are means ± s.e.m. ($n = 3$ independent experiments). (C, D) Huh-7 cells were co-transduced with AAV vectors encoding *Spy*Cas9, a sgRNA targeting the human CCR5 (**C**) or AAVS1 (**D**) locus and the indicated AcrIIA4 variant, followed by T7 endonuclease assay. During transduction, the Acr vector dose was varied as indicated. Data are means ± s.e.m. ($n = 3$ independent experiments). (A–D) n.s. = not significant, $^*P < 0.05$, $^{**}P < 0.01$, $^{***}P < 0.001$, by two-sided Student's *t*-test with Bonferroni correction. Precise *P*-values are shown in Table 1 (Material and Methods). (**E**) Schematic of AcrIIA4 vectors for cardiomyocyte-specific genome editing. (F, G) MiR-1-dependent indel mutation of the Rosa-26 locus in cardiomyocytes. HL-1 cells were co-transduced with AAV vectors expressing *Spy*Cas9, a sgRNA targeting the murine Rosa-26 locus, and AcrIIA4 either with or without miR-1 binding sites, followed by TIDE sequencing. (**F**) Detailed analysis of indels observed at the Rosa-26 locus. Data for a representative sample is shown. (**G**) Quantification of the overall editing efficiency. Data are means ± s.e.m. ($n = 3$ independent experiments).

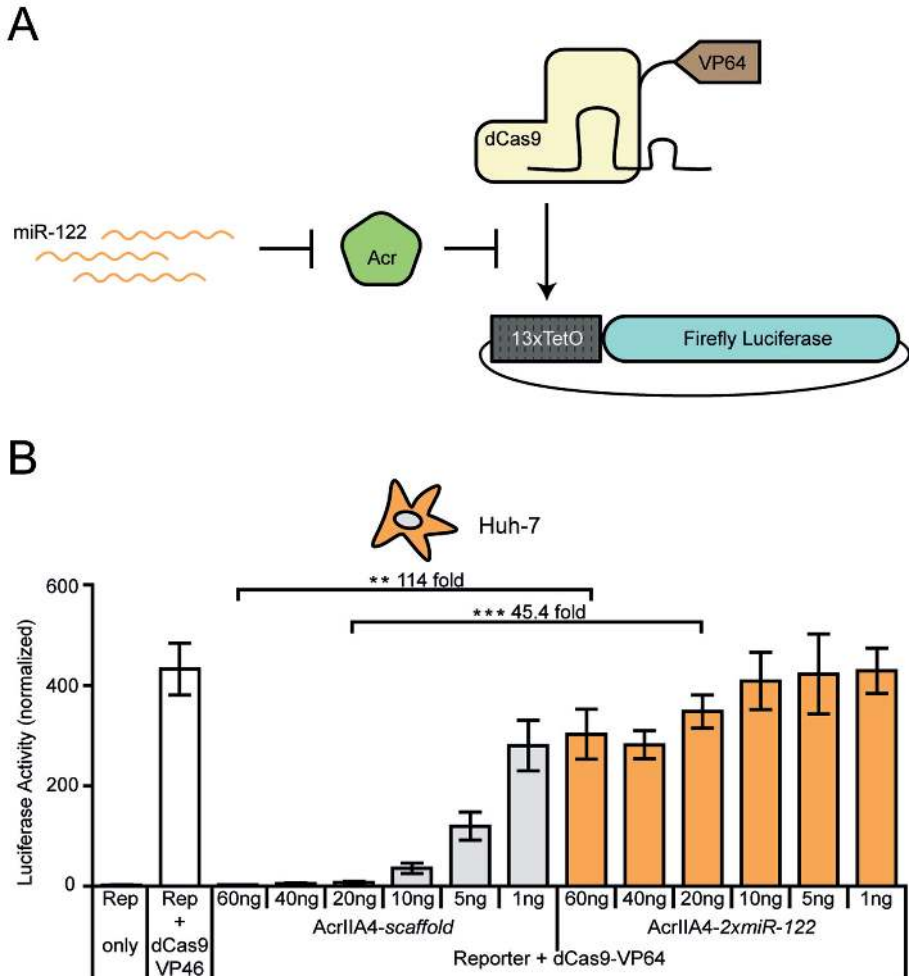

Figure 3. MiR-122-dependent gene activation via *Spy*dCas9-VP64. (**A**) Schematic of miR-122-dependent activation of luciferase reporter expression. MiR-122-dependent knockdown of AcrIIA4 results in *Spy*dCas9-VP64 activity and thus luciferase expression. (**B**) Huh-7 cells were co-transfected with vectors encoding *Spy*dCas9-VP64, a luciferase reporter driven by a minimal promoter preceded by tet operator (TetO) sites, a TetO-targeting sgRNA and AcrIIA4-*miR-122* or AcrIIA4-*scaffold* construct (as control), followed by a luciferase assay. During transduction, the Acr vector dose was varied as indicated. Data are means ± s.e.m. ($n = 4$ independent experiments). $^{**}P < 0.01$, $^{***}P < 0.001$, by two-sided Student's *t*-test with Bonferroni correction. For all doses, precise *P*-values are shown in Table 1 (Material and Methods).

plasmids encoding the N- and C-terminal *Spy*Cas9 fragments alongside an AcrIIA4 vector (with or without miR-122 sites in the 3′UTR) and the aforementioned luciferase cleavage reporter into Huh-7 cells (or HeLa cells as control). In Huh-7 cells, the split-*Spy*Cas9 remained fully active in the presence of the AcrIIA4-*2xmiR-122* vector as indicated by potent luciferase knockdown, but was completely impaired if we co-administered the AcrIIA4-*scaffold* construct (Supplementary Figure S8). In HeLa cells, in contrast, split-*Spy*Cas9 activity was impaired upon co-delivery of both, the AcrIIA4-*2xmiR-122* or the AcrIIA4-*scaffold* vector (Supplementary Figure S8), demonstrating that our Cas9-ON switch can also be applied to control split-*Spy*Cas9.

MiR-1 plays an important role in muscle cell differentiation (22,23) and remains highly expressed in mature muscle cells (53). Using a luciferase knockdown assay, we confirmed high miR-1 levels in HL-1 cells, a widely employed murine cardiac muscle cell model (Supplementary Figure S9). We hypothesized that, similarly to miR-122 in hepatocytes, miR-1 could be harnessed to render CRISPR–Cas9 activity cardiomyocyte-specific using the identical, Acr-based strategy. We therefore exchanged the two miR-122 binding sites in our AcrIIA4 constructs by two miR-1 target sites (Figure 2E).

Then, we packaged the resulting AcrIIA4-*2xmiR-1* construct or the AcrIIA4-*scaffold* construct (as control), a *Spy*Cas9 transgene, and a sgRNA targeting the murine Rosa-26 locus into AAV serotype 6, which is known to efficiently transduce a wide spectrum of tissues *in vitro and vivo*, including myocytes (54–56). Upon co-infection of HL-1 cells with these vectors, we observed potent editing of the Rosa-26 locus in the presence of the AcrIIA4-*2xmiR-1* vector, but not when using the AcrIIA4-*scaffold* control vector (Figure 2F, G and Supplementary Figure S10), demonstrating miR-1-dependent *Spy*Cas9 activity in cardiomyocytes.

To investigate whether the aforementioned miR-122- and miR-1-based Cas-ON switches are orthogonal, we overexpressed miR-122 or miR-1 in HEK293T cells not naturally expressing either of these miRNAs (Supplementary Figure

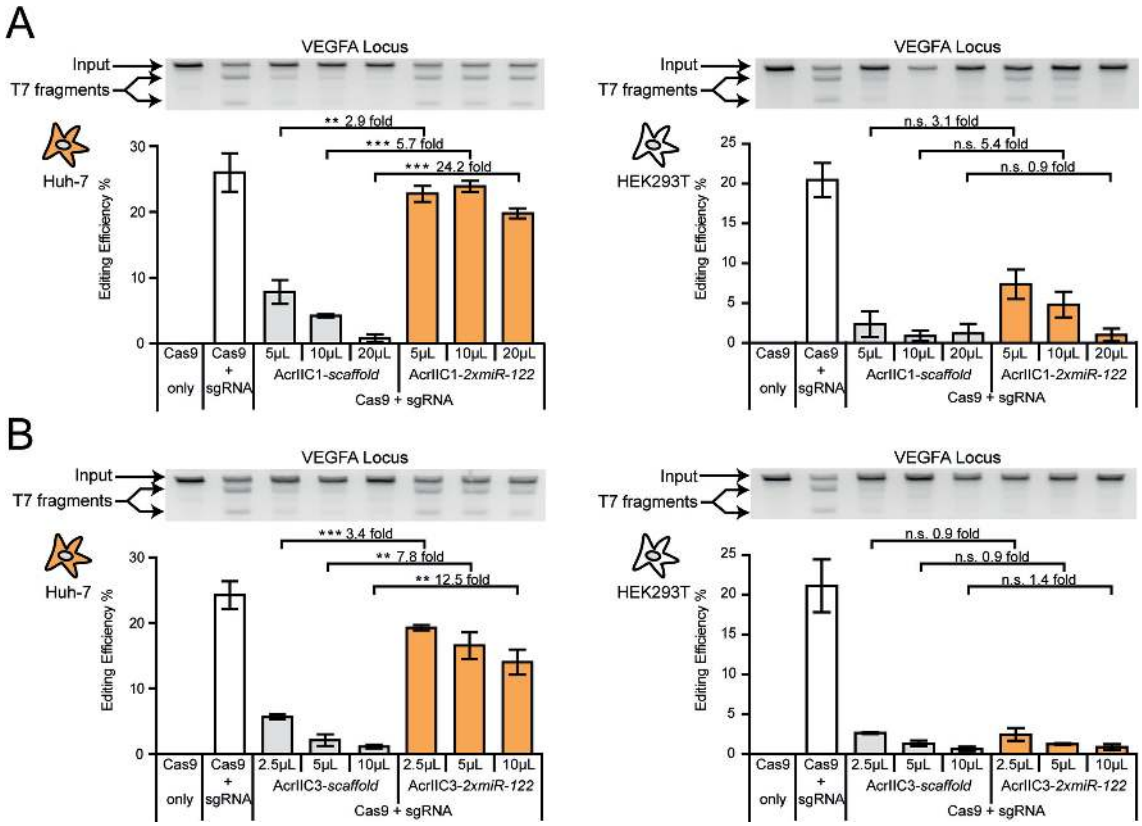

Figure 4. Hepatocyte-specific *Nme*Cas9 activity. (A, B) Huh-7 or HEK293T cells were co-transduced with AAV vectors expressing *Nme*Cas9, a sgRNA targeting the human VEGFA locus and either AcrIIC1 (**A**) or AcrIIC3 (**B**) carrying two miR-122 target sites or not, followed by T7 endonuclease assay. During transduction, the Acr vector dose was varied as indicated. Data are means ± s.e.m. ($n = 3$ independent experiments). n.s. = not significant, $^{**}P < 0.01$, $^{***}P < 0.001$, by two-sided Student's *t*-test with Bonferroni correction. Precise *P*-values are shown in Table 1 (Materials and Methods).

S11A). Acr knockdown and concurrent release of Cas9 activity were only observed when the miR-1- and miR-122-dependent Acrs were co-transfected with their matching miRNA expression vectors (Supplementary Figure S11B–D), demonstrating that our Cas-ON switches are selective with respect to the miRNA trigger.

miRNA control of dCas9-effector fusions

So far, we have demonstrated the power of our Cas9-ON system for cell type-specific genome editing. However, the CRISPR–Cas9 system offers many applications that go beyond a targeted introduction of double-strand breaks. These are typically based on catalytically inactive d(ead)Cas9 mutants employed as programmable DNA binding domain to recruit effector domains to selected genomic loci. These effectors then mediate e.g. transcriptional activation or repression (6–8,57–59), epigenetic modification (9–11,60,61) or base editing (12,13,62). AcrIIA4 inhibits the *Spy*Cas9 mainly by blocking its DNA binding (31,63). We therefore hypothesized that our miRNA-dependent *Spy*Cas9-ON switch should also be applicable to *Spy*dCas9-effector fusions.

To test this hypothesis, we co-transfected vectors encoding a *Spy*dCas9-VP64 transcriptional activator, a Tet operator (TetO) targeting sgRNA, a luciferase reporter driven from a TetO-dependent promoter, and an AcrIIA4-*2xmiR-122* or AcrIIA4-*scaffold* vector into Huh-7 cells (Figure 3A). We observed a potent, miR-122-dependent luciferase reporter activation with a maximum dynamic range of regulation of 114-fold (for the 60 ng dose, *P*-value = 0.008; Figure 3B). Remarkably, the leakiness and dynamic range of the system could be tuned over a wide range by varying the AcrIIA4 vector dose (Figure 3B). These results illustrate that our *Spy*Cas9-ON system can also be applied on *Spy*dCas9-effector fusions.

Hepatocyte-specific genome editing with *Nme*Cas9

Although the *Spy*Cas9 remains the most widely employed CRISPR–Cas orthologue, the ongoing discovery and characterization of novel CRISPR–Cas effectors from various species rapidly expands the CRISPR toolbox. For many of these novel type I and II CRISPR–Cas effectors, corresponding anti-CRISPR proteins have already been found or are likely to be discovered in the near future (28–30,42,44,64,65), suggesting that our Cas9-ON approach might be easily transferable to many other CRISPR–Cas orthologues. One such orthologue is the *Neisseria meningitidis* (*Nme*)Cas9, which is not only ∼300 amino acids smaller than *Spy*Cas9, but also shows a far lower activity on off-target loci, presumably due to its extended protospacer sequence (66–68). Two anti-CRISPR proteins have recently been described, which efficiently inhibit *Nme*Cas9 via dis-

tinct mechanisms. AcrIIC1 perturbs the *Nme*Cas9 nuclease function, while AcrIIC3 induces *Nme*Cas9 dimerization, thereby impairing its DNA binding (29,32).

We speculated that, similar to *Spy*Cas9 control via miR-dependent AcrIIA4, placing AcrIIC1 and AcrIIC3 under miRNA regulation would enable cell-specific *Nme*Cas9 activity. To test this hypothesis, we codon-optimized the AcrIIC1 and AcrIIC3 genes, introduced miR-122 target sites into their 3′UTRs and packaged them into AAV2. Then, we co-transduced Huh-7 or HEK293T control cells with the AcrIIC1-*2xmiR-122* or AcrIIC3-*2xmiR-122* vector (or AcrIIC1-*scaffold* or AcrIIC3-*scaffold* as control) alongside a vector co-encoding *Nme*Cas9 and a sgRNA targeting the human VEGFA locus (39,69). As hoped for, we observed potent miR-122-dependent indel mutation of the VEGFA target locus with an up to 24-fold dynamic range of miRNA-regulation depending on the vector dose (20 μl AcrIIC1 dose; P-value < 0.0001; Figure 4 and Supplementary Figure S12). In HEK293T control cells, in contrast, *Nme*Cas9 inhibition was independent of the presence of miR-122 target sites on the Acr vectors (Figure 4), demonstrating that our Cas-ON switch can confine *Nme*Cas9 activity to selected cell types.

DISCUSSION

CRISPR–Cas technologies enable detailed genetic studies in cells and animals and hold unmet potential for the treatment of genetic disorders. To render CRISPR–Cas *in vivo* applications as specific and thus as safe as possible, strategies to confine the activity of Cas9 nucleases or dCas9-based effectors to defined cells and tissues are highly desired.

In this study, we employed cellular miRNA signatures to control the expression of anti-CRISPR proteins, thereby creating a synthetic circuit limiting Cas9 activity to selected target cells.

Liver and muscle are interesting target tissues for CRISPR-mediated gene therapy approaches, e.g. for treatment of hemophilia or Duchenne muscular dystrophy, respectively (70–74). Using our Cas9-ON system, we were able to confine CRISPR–Cas9 activity selectively to hepatocytes or cardiomyocytes by employing miR-122 and miR-1 as cellular markers, respectively, while efficiently inhibiting Cas9 in unrelated cell types lacking these markers (HeLa and HEK293T). A recent study estimated 222 miRNAs to be specifically enriched within selected tissues (75), e.g. hematopoietic cells (miR-142 (24,76,77)) or neurons (e.g. miR-376a, miR-434 (78)). Thus, we anticipate that our Cas9-ON strategy will be highly versatile. Apart from the cell-type specificity of miRNAs, users of our technology should also consider the total level of miRNA expression within target cells when choosing miRNA triggers to be combined with our Cas-ON switch. For instance, miRNAs that are highly cell type-specific but only expressed at relatively low levels are unlikely to enable efficient Acr knockdown. In such cases, incorporating target sites for multiple, specific miRNAs into the *acr* transgene 3′UTR might be required to achieve the desired level of Cas9 activity and control.

Our anti-CRISPR-based Cas-ON system has several advantages as compared to the Cas-ON switch by Hirosawa *et al.*, which is based on a translational negative-feedback loop mediated by an L7Ae repressor (27). When simultaneously delivering the L7Ae-, K-turn-Cas9- and sgRNA-encoding constructs, substantial amounts of Cas9-sgRNA complexes will be made by the cells before the L7Ae can accumulate in sufficient quantities to block Cas9 translation. This results in considerable leakiness, i.e. ∼60% of Cas9 activity in the OFF state (27). Our Cas-ON switch design overcomes this essential limitation by establishing a post-translational negative-feedback loop based on anti-CRISPR proteins. Upon co-delivery of vectors encoding Cas9, sgRNA and Acr, the anti-CRISPR proteins will be made in parallel to Cas9 and the sgRNA. Due to the high affinity of Acrs to Cas9–sgRNA complexes (79,80), this switch design is tighter than the previous system (27). In fact, we showed that by increasing Acr vector doses, Cas9 activity in the OFF state can be pushed towards the detection limits of the used assays (Figures 2A–D, 3 and 4). However, at very high Acr doses, we also observed noticeable suppression of CRISPR–Cas9 activity even in the ON state. This is most likely due to the limited capacity of the RNAi machinery (36), which is unable to fully knock down Acr expression in ON-target cells when Acr transcript levels exceed a certain limit (Supplementary Figure S7). In contrast, very low Acr vector doses led to insufficient Acr expression in the OFF state (Supplementary Figure S7) and resulted in considerable Cas9 activity even in off-target cells. By modulating the dose of the supplied Acr vector or the strength of the Acr-driving promoter, one can tune the system towards the desired switching behavior for a specific application.

Of note, across T7 experiments, we found the overall editing efficiencies in the used control cell lines (HEK293T and HeLa) to be slightly lower as compared to Huh-7 (Figures 2B and 4). As these differences in editing efficiencies did not correlate with transduction efficiencies (Supplementary Figure S5), we speculate that they might result from differences in promoter strength (81), chromatin status at the targeted loci and/or timing, as well as efficiency of double-stranded DNA break repair by non-homologous end-joining.

A particularly important feature of our Cas9-ON switch is its modularity, i.e. it should be compatible with any Cas9 orthologue, for which a potent anti-CRISPR protein is known (as exemplified here for *Spy*Cas9 and *Nme*Cas9). In light of the ongoing, rapid discovery and characterization of novel Acrs, the application spectrum of our switch is likely to further expand in the near future. Importantly, our Cas-ON strategy is also applicable to dCas9-effector fusions, provided an Acr is employed, which impairs Cas9 DNA binding. This is the case, e.g. for AcrIIA4 and AcrIIC3, which block DNA targeting of *Spy*Cas9 and *Nme*Cas9, respectively, but not for AcrIIC1, which impairs the *Nme*Cas9 nuclease function, but does not interfere with its DNA binding. Therefore, the underlying, inhibitory mechanism can be an important parameter to consider when selecting Acrs to be used in our Cas-ON system.

Importantly, our Cas-ON switch is compatible with many existing strategies for tissue-specific gene delivery and expression, such as engineered or evolved AAV vectors (45,46,82) or tissue-specific promoters (83,84). Thus, combining these approaches, potentially with additional layers

of CRISPR–Cas control via chemical triggers (48,85,86) or light (34,50,87,88), will likely enable highly specific genome perturbations.

While we foresee that the most relevant applications of our approach will be in animal models and, in the long run, potentially in human patients, we reckon that a careful investigation of toxicity or immune reactions that might result from Acr overexpression should precede *in vivo* translation of our Cas9-ON strategy. Moreover, to avoid continuous sequestration of the endogenous miRNA pool within the target cells, it could be advisable to couple our Cas9-ON strategy to vector self-inactivation (89).

Taken together, our work demonstrates the power of miRNA-dependent anti-CRISPR transgenes to confine CRISPR–Cas9 activity to selected cells types and facilitate safe and precise genome perturbations in animals and patients.

DATA AVAILABILITY

Vectors are available via Addgene (#120293 - 120303). Annotated sequences (GenBank files) of all vectors created in this study are provided as Supplementary data. Flow cytometry data is available on FlowRepository (Repository ID: FR-FCM-ZYVK).

SUPPLEMENTARY DATA

Supplementary Data are available at NAR Online.

ACKNOWLEDGEMENTS

We thank the Synthetic Biology group (Heidelberg University), the Virus-Host Interactions group (University Heidelberg, Hospital) and the Intelligent Imaging group (DKFZ, Heidelberg) for helpful discussions, K. Rippe (DKFZ, Heidelberg) and E. Wiedtke (University Hospital, Heidelberg) for providing cell lines, and J. Notbohm and A. Bietz (both University Heidelberg) for testing the VEGFA sgRNA. We are further grateful to Moritoshi Sato (University of Tokyo), Feng Zhang (Massachusetts Institute of Technology, Cambridge), George Church (Harvard University, Cambridge), and Erik J. Sontheimer (University of Massachusetts Medical School, Worcester) for sharing plasmids as well as Monika Langlotz and the ZMBH FACS core facility (University Heidelberg) for support with FACS measurements.

Author contributions: D.G. and D.N. conceived the study. M.D.H. and D.N. designed experiments. M.D.H., S.A., S.G., K.R., M.M. and K.B. conducted experiments. M.D.H. and D.N. analyzed and interpreted data. J.F. developed the luciferase cleavage reporter construct. D.G. provided expertise for AAV experiments and CRISPR assays. C.D. made practical contributions. R.E., D.G. and D.N. jointly directed the work. M.D.H., D.G. and D.N. wrote the manuscript with support from all authors.

FUNDING

Helmholtz association, the German Research Foundation (DFG); Federal Ministry of Education and Research (BMBF); Helmholtz International Graduate School for Cancer Research scholarship (DKFZ, Heidelberg to M.D.H.); German Center for Infection Research (DZIF, BMBF) [TTU 04.830 and 04.815 to K.B. and D.G.]; Cystic Fibrosis Foundation (CFF) [GRIMM15XX0 to J.F. and D.G.]; Transregional Collaborative Research Center TRR179 (DFG; TP18 to D.G. and Z2 to R.E.) [272983813 D.G. and R.E.]; D.G. acknowledges additional funding by the Collaborative Research Center SFB1129 (DFG; TP2 [2014–2018] and TP16 [2018–2022]) [2402455660]; Cluster of Excellence CellNetworks (DFG) [EXC81]. D.G. and C.D. participate in the SMART-HaemoCare consortium, which receives financial support from ERA-NET E-Rare-3 [JCT-2015)/DFG]. K.R. was partially supported by the Marie Curie International Incoming Fellowship [PIIF-GA-2013-627329]. Funding for open access charge: German Research Council (DFG).

Conflict of interest statement. D.N., D.G., R.E., M.D.H., J.F., C.D. and S.A. have filed patent applications related to this work.

REFERENCES

1. Jinek,M., East,A., Cheng,A., Lin,S., Ma,E. and Doudna,J. (2013) RNA-programmed genome editing in human cells. *Elife*, **2**, e00471.
2. Cong,L., Ran,F.A., Cox,D., Lin,S., Barretto,R., Habib,N., Hsu,P.D., Wu,X., Jiang,W., Marraffini,L.A. *et al.* (2013) Multiplex genome engineering using CRISPR/Cas systems. *Science*, **339**, 819–823.
3. Mali,P., Yang,L., Esvelt,K.M., Aach,J., Guell,M., DiCarlo,J.E., Norville,J.E. and Church,G.M. (2013) RNA-guided human genome engineering via Cas9. *Science*, **339**, 823–826.
4. Cho,S.W., Kim,S., Kim,J.M. and Kim,J.S. (2013) Targeted genome engineering in human cells with the Cas9 RNA-guided endonuclease. *Nat. Biotechnol.*, **31**, 230–232.
5. Hsu,P.D., Lander,E.S. and Zhang,F. (2014) Development and applications of CRISPR–Cas9 for genome engineering. *Cell*, **157**, 1262–1278.
6. Qi,L.S., Larson,M.H., Gilbert,L.A., Doudna,J.A., Weissman,J.S., Arkin,A.P. and Lim,W.A. (2013) Repurposing CRISPR as an RNA-guided platform for sequence-specific control of gene expression. *Cell*, **152**, 1173–1183.
7. Maeder,M.L., Linder,S.J., Cascio,V.M., Fu,Y., Ho,Q.H. and Joung,J.K. (2013) CRISPR RNA-guided activation of endogenous human genes. *Nat. Methods*, **10**, 977–979.
8. Konermann,S., Brigham,M.D., Trevino,A.E., Joung,J., Abudayyeh,O.O., Barcena,C., Hsu,P.D., Habib,N., Gootenberg,J.S., Nishimasu,H. *et al.* (2015) Genome-scale transcriptional activation by an engineered CRISPR–Cas9 complex. *Nature*, **517**, 583–588.
9. Stepper,P., Kungulovski,G., Jurkowska,R.Z., Chandra,T., Krueger,F., Reinhardt,R., Reik,W., Jeltsch,A. and Jurkowski,T.P. (2017) Efficient targeted DNA methylation with chimeric dCas9-Dnmt3a-Dnmt3L methyltransferase. *Nucleic Acids Res.*, **45**, 1703–1713.
10. Hilton,I.B., D'Ippolito,A.M., Vockley,C.M., Thakore,P.I., Crawford,G.E., Reddy,T.E. and Gersbach,C.A. (2015) Epigenome editing by a CRISPR–Cas9-based acetyltransferase activates genes from promoters and enhancers. *Nat. Biotechnol.*, **33**, 510–517.
11. Vojta,A., Dobrinic,P., Tadic,V., Bockor,L., Korac,P., Julg,B., Klasic,M. and Zoldos,V. (2016) Repurposing the CRISPR–Cas9 system for targeted DNA methylation. *Nucleic Acids Res.*, **44**, 5615–5628.
12. Komor,A.C., Kim,Y.B., Packer,M.S., Zuris,J.A. and Liu,D.R. (2016) Programmable editing of a target base in genomic DNA without double-stranded DNA cleavage. *Nature*, **533**, 420–424.
13. Gaudelli,N.M., Komor,A.C., Rees,H.A., Packer,M.S., Badran,A.H., Bryson,D.I. and Liu,D.R. (2017) Programmable base editing of A*T to G*C in genomic DNA without DNA cleavage. *Nature*, **551**, 464–471.
14. Cox,D.B., Platt,R.J. and Zhang,F. (2015) Therapeutic genome editing: prospects and challenges. *Nat. Med.*, **21**, 121–131.

15. Dai,W.J., Zhu,L.Y., Yan,Z.Y., Xu,Y., Wang,Q.L. and Lu,X.J. (2016) CRISPR–Cas9 for in vivo Gene Therapy: Promise and Hurdles. *Mol. Ther. Nucleic Acids*, **5**, e349.
16. Gebert,L.F.R. and MacRae,I.J. (2018) Regulation of microRNA function in animals. *Nat. Rev. Mol. Cell Biol.*, **20**, 21–37.
17. He,L. and Hannon,G.J. (2004) MicroRNAs: small RNAs with a big role in gene regulation. *Nat. Rev. Genet.*, **5**, 522–531.
18. Lagos-Quintana,M., Rauhut,R., Yalcin,A., Meyer,J., Lendeckel,W. and Tuschl,T. (2002) Identification of tissue-specific microRNAs from mouse. *Curr. Biol.*, **12**, 735–739.
19. Amirkhah,R., Meshkin,H.N., Farazmand,A., Rasko,J.E.J. and Schmitz,U. (2017) Computational and experimental identification of Tissue-Specific MicroRNA targets. *Methods Mol. Biol.*, **1580**, 127–147.
20. Medina,P.P., Nolde,M. and Slack,F.J. (2010) OncomiR addiction in an in vivo model of microRNA-21-induced pre-B-cell lymphoma. *Nature*, **467**, 86–90.
21. He,C., Luo,B., Jiang,N., Liang,Y., He,Y., Zeng,J., Liu,J. and Zheng,X. (2018) OncomiR or antioncomiR: Role of miRNAs in acute myeloid leukemia. *Leuk. Lymphoma*, **6**, 1–12.
22. Chen,J.F., Mandel,E.M., Thomson,J.M., Wu,Q., Callis,T.E., Hammond,S.M., Conlon,F.L. and Wang,D.Z. (2006) The role of microRNA-1 and microRNA-133 in skeletal muscle proliferation and differentiation. *Nat. Genet.*, **38**, 228–233.
23. Horak,M., Novak,J. and Bienertova-Vasku,J. (2016) Muscle-specific microRNAs in skeletal muscle development. *Dev. Biol.*, **410**, 1–13.
24. Brown,B.D., Venneri,M.A., Zingale,A., Sergi Sergi,L. and Naldini,L. (2006) Endogenous microRNA regulation suppresses transgene expression in hematopoietic lineages and enables stable gene transfer. *Nat. Med.*, **12**, 585–591.
25. Amendola,M., Giustacchini,A., Gentner,B. and Naldini,L. (2013) A double-switch vector system positively regulates transgene expression by endogenous microRNA expression (miR-ON vector). *Mol. Ther.*, **21**, 934–946.
26. Senís,E., Fatouros,C., Große,S., Wiedtke,E., Niopek,D., Mueller,A.-K., Börner,K. and Grimm,D. (2014) CRISPR/Cas9-mediated genome engineering: An adeno-associated viral (AAV) vector toolbox. *Biotechnol. J.*, **9**, 1402–1412.
27. Hirosawa,M., Fujita,Y., Parr,C.J.C., Hayashi,K., Kashida,S., Hotta,A., Woltjen,K. and Saito,H. (2017) Cell-type-specific genome editing with a microRNA-responsive CRISPR–Cas9 switch. *Nucleic Acids Res.*, **45**, e118.
28. Bondy-Denomy,J., Pawluk,A., Maxwell,K.L. and Davidson,A.R. (2013) Bacteriophage genes that inactivate the CRISPR/Cas bacterial immune system. *Nature*, **493**, 429–432.
29. Pawluk,A., Amrani,N., Zhang,Y., Garcia,B., Hidalgo-Reyes,Y., Lee,J., Edraki,A., Shah,M., Sontheimer,E.J., Maxwell,K.L. *et al.* (2016) Naturally occurring Off-Switches for CRISPR–Cas9. *Cell*, **167**, 1829–1838.
30. Rauch,B.J., Silvis,M.R., Hultquist,J.F., Waters,C.S., McGregor,M.J., Krogan,N.J. and Bondy-Denomy,J. (2016) Inhibition of CRISPR–Cas9 with bacteriophage proteins. *Cell*, **168**, 150–158.
31. Dong, Guo,M., Wang,S., Zhu,Y., Wang,S., Xiong,Z., Yang,J., Xu,Z. and Huang,Z. (2017) Structural basis of CRISPR-SpyCas9 inhibition by an anti-CRISPR protein. *Nature*, **546**, 436–439.
32. Harrington,L.B., Doxzen,K.W., Ma,E., Liu,J.J., Knott,G.J., Edraki,A., Garcia,B., Amrani,N., Chen,J.S., Cofsky,J.C. *et al.* (2017) A Broad-Spectrum inhibitor of CRISPR–Cas9. *Cell*, **170**, 1224–1233.
33. Engler,C., Kandzia,R. and Marillonnet,S. (2008) A one pot, one step, precision cloning method with high throughput capability. *PLoS One*, **3**, e3647.
34. Bubeck,F., Hoffmann,M.D., Harteveld,Z., Aschenbrenner,S., Bietz,A., Waldhauer,M.C., Borner,K., Fakhiri,J., Schmelas,C., Dietz,L. *et al.* (2018) Engineered anti-CRISPR proteins for optogenetic control of CRISPR–Cas9. *Nat. Methods*, **15**, 924–927.
35. Chen,B., Gilbert,L.A., Cimini,B.A., Schnitzbauer,J., Zhang,W., Li,G.W., Park,J., Blackburn,E.H., Weissman,J.S., Qi,L.S. *et al.* (2013) Dynamic imaging of genomic loci in living human cells by an optimized CRISPR/Cas system. *Cell*, **155**, 1479–1491.
36. Borner,K., Niopek,D., Cotugno,G., Kaldenbach,M., Pankert,T., Willemsen,J., Zhang,X., Schurmann,N., Mockenhaupt,S., Serva,A. *et al.* (2013) Robust RNAi enhancement via human Argonaute-2 overexpression from plasmids, viral vectors and cell lines. *Nucleic Acids Res.*, **41**, e199.
37. Fakhiri,J., Schneider,M.A., Puschhof,J., Stanifer,M., Schildgen,V., Holderbach,S., Voss,Y., El Andari,J., Schildgen,O., Boulant,S. *et al.* (2019) Novel chimeric gene therapy vectors based on Adeno-Associated virus and four different mammalian bocaviruses. *Mol. Ther. Methods Clin. Dev.*, **12**, 202–222.
38. Schurmann,N., Trabuco,L.G., Bender,C., Russell,R.B. and Grimm,D. (2013) Molecular dissection of human Argonaute proteins by DNA shuffling. *Nat. Struct. Mol. Biol.*, **20**, 818–826.
39. Amrani,N., Gao,X.D., Liu,P., Edraki,A., Mir,A., Ibraheim,R., Gupta,A., Sasaki,K.E., Wu,T., Donohoue,P.D. *et al.* (2018) NmeCas9 is an intrinsically high-fidelity genome-editing platform. *Genome Biol.*, **19**, 214.
40. Borner,K., Hermle,J., Sommer,C., Brown,N.P., Knapp,B., Glass,B., Kunkel,J., Torralba,G., Reymann,J., Beil,N. *et al.* (2010) From experimental setup to bioinformatics: an RNAi screening platform to identify host factors involved in HIV-1 replication. *Biotechnol. J.*, **5**, 39–49.
41. Brinkman,E.K., Chen,T., Amendola,M. and van Steensel,B. (2014) Easy quantitative assessment of genome editing by sequence trace decomposition. *Nucleic Acids Res.*, **42**, e168.
42. Pawluk,A., Bondy-Denomy,J., Cheung,V.H., Maxwell,K.L. and Davidson,A.R. (2014) A new group of phage anti-CRISPR genes inhibits the type I-E CRISPR–Cas system of Pseudomonas aeruginosa. *MBio.*, **5**, e00896.
43. Bondy-Denomy,J., Garcia,B., Strum,S., Du,M., Rollins,M.F., Hidalgo-Reyes,Y., Wiedenheft,B., Maxwell,K.L. and Davidson,A.R. (2015) Multiple mechanisms for CRISPR–Cas inhibition by anti-CRISPR proteins. *Nature*, **526**, 136–139.
44. Hynes,A.P., Rousseau,G.M., Lemay,M.L., Horvath,P., Romero,D.A., Fremaux,C. and Moineau,S. (2017) An anti-CRISPR from a virulent streptococcal phage inhibits Streptococcus pyogenes Cas9. *Nat. Microbiol.*, **2**, 1374–1380.
45. Grimm,D. and Buning,H. (2017) Small but increasingly mighty: latest advances in AAV vector research, design, and evolution. *Hum. Gene Ther.*, **28**, 1075–1086.
46. Grimm,D., Lee,J.S., Wang,L., Desai,T., Akache,B., Storm,T.A. and Kay,M.A. (2008) In vitro and in vivo gene therapy vector evolution via multispecies interbreeding and retargeting of adeno-associated viruses. *J. Virol.*, **82**, 5887–5911.
47. Kienle,E., Senis,E., Borner,K., Niopek,D., Wiedtke,E., Grosse,S. and Grimm,D. (2012) Engineering and evolution of synthetic adeno-associated virus (AAV) gene therapy vectors via DNA family shuffling. *J. Vis. Exp.*, e3819.
48. Zetsche,B., Volz,S.E. and Zhang,F. (2015) A split-Cas9 architecture for inducible genome editing and transcription modulation. *Nat. Biotechnol.*, **33**, 139–142.
49. Wright,A.V., Sternberg,S.H., Taylor,D.W., Staahl,B.T., Bardales,J.A., Kornfeld,J.E. and Doudna,J.A. (2015) Rational design of a split-Cas9 enzyme complex. *Proc. Natl. Acad. Sci. U.S.A.*, **112**, 2984–2989.
50. Nihongaki,Y., Kawano,F., Nakajima,T. and Sato,M. (2015) Photoactivatable CRISPR–Cas9 for optogenetic genome editing. *Nat. Biotechnol.*, **33**, 755–760.
51. Truong,D.J., Kuhner,K., Kuhn,R., Werfel,S., Engelhardt,S., Wurst,W. and Ortiz,O. (2015) Development of an intein-mediated split-Cas9 system for gene therapy. *Nucleic Acids Res.*, **43**, 6450–6458.
52. Chew,W.L., Tabebordbar,M., Cheng,J.K., Mali,P., Wu,E.Y., Ng,A.H., Zhu,K., Wagers,A.J. and Church,G.M. (2016) A multifunctional AAV-CRISPR–Cas9 and its host response. *Nat. Methods*, **13**, 868–874.
53. Lamon,S., Zacharewicz,E., Butchart,L.C., Orellana,L., Mikovic,J., Grounds,M.D. and Russell,A.P. (2017) MicroRNA expression patterns in post-natal mouse skeletal muscle development. *BMC Genomics*, **18**, 52.
54. Arnett,A.L., Konieczny,P., Ramos,J.N., Hall,J., Odom,G., Yablonka-Reuveni,Z., Chamberlain,J.R. and Chamberlain,J.S. (2014) Adeno-associated viral (AAV) vectors do not efficiently target muscle satellite cells. *Mol. Ther. Methods Clin. Dev.*, **1**, 14038.
55. Sipo,I., Fechner,H., Pinkert,S., Suckau,L., Wang,X., Weger,S. and Poller,W. (2007) Differential internalization and nuclear uncoating of self-complementary adeno-associated virus pseudotype vectors as determinants of cardiac cell transduction. *Gene Ther.*, **14**, 1319–1329.
56. Ellis,B.L., Hirsch,M.L., Barker,J.C., Connelly,J.P., Steininger,R.J. 3rd and Porteus,M.H. (2013) A survey of ex vivo/in vitro transduction efficiency of mammalian primary cells and cell lines with Nine

natural adeno-associated virus (AAV1-9) and one engineered adeno-associated virus serotype. *Virol. J.*, **10**, 74.
57. Perez-Pinera,P., Kocak,D.D., Vockley,C.M., Adler,A.F., Kabadi,A.M., Polstein,L.R., Thakore,P.I., Glass,K.A., Ousterout,D.G., Leong,K.W. *et al.* (2013) RNA-guided gene activation by CRISPR–Cas9-based transcription factors. *Nat. Methods*, **10**, 973–976.
58. Tanenbaum,M.E., Gilbert,L.A., Qi,L.S., Weissman,J.S. and Vale,R.D. (2014) A protein-tagging system for signal amplification in gene expression and fluorescence imaging. *Cell*, **159**, 635–646.
59. Mali,P., Aach,J., Stranges,P.B., Esvelt,K.M., Moosburner,M., Kosuri,S., Yang,L. and Church,G.M. (2013) CAS9 transcriptional activators for target specificity screening and paired nickases for cooperative genome engineering. *Nat. Biotechnol.*, **31**, 833–838.
60. Kearns,N.A., Pham,H., Tabak,B., Genga,R.M., Silverstein,N.J., Garber,M. and Maehr,R. (2015) Functional annotation of native enhancers with a Cas9-histone demethylase fusion. *Nat. Methods*, **12**, 401–403.
61. Thakore,P.I., D'Ippolito,A.M., Song,L., Safi,A., Shivakumar,N.K., Kabadi,A.M., Reddy,T.E., Crawford,G.E. and Gersbach,C.A. (2015) Highly specific epigenome editing by CRISPR–Cas9 repressors for silencing of distal regulatory elements. *Nat. Methods*, **12**, 1143–1149.
62. Hess,G.T., Tycko,J., Yao,D. and Bassik,M.C. (2017) Methods and applications of CRISPR-Mediated base editing in eukaryotic genomes. *Mol. Cell*, **68**, 26–43.
63. Yang,H. and Patel,D.J. (2017) Inhibition mechanism of an Anti-CRISPR suppressor AcrIIA4 targeting SpyCas9. *Mol. Cell*, **67**, 117–127.
64. Pawluk,A., Staals,R.H., Taylor,C., Watson,B.N., Saha,S., Fineran,P.C., Maxwell,K.L. and Davidson,A.R. (2016) Inactivation of CRISPR–Cas systems by anti-CRISPR proteins in diverse bacterial species. *Nat. Microbiol.*, **1**, 16085.
65. Hynes,A.P., Rousseau,G.M., Agudelo,D., Goulet,A., Amigues,B., Loehr,J., Romero,D.A., Fremaux,C., Horvath,P., Doyon,Y. *et al.* (2018) Widespread anti-CRISPR proteins in virulent bacteriophages inhibit a range of Cas9 proteins. *Nat. Commun.*, **9**, 2919.
66. Esvelt,K.M., Mali,P., Braff,J.L., Moosburner,M., Yaung,S.J. and Church,G.M. (2013) Orthogonal Cas9 proteins for RNA-guided gene regulation and editing. *Nat. Methods*, **10**, 1116.
67. Hou,Z., Zhang,Y., Propson,N.E., Howden,S.E., Chu,L.F., Sontheimer,E.J. and Thomson,J.A. (2013) Efficient genome engineering in human pluripotent stem cells using Cas9 from Neisseria meningitidis. *Proc. Natl. Acad. Sci. U.S.A.*, **110**, 15644–15649.
68. Lee,C.M., Cradick,T.J. and Bao,G. (2016) The neisseria meningitidis CRISPR–Cas9 system enables specific genome editing in mammalian cells. *Mol. Ther.*, **24**, 645–654.
69. Ibraheim,R., Song,C.-Q., Mir,A., Amrani,N., Xue,W. and Sontheimer,E.J. (2018) All-in-one adeno-associated virus delivery and genome editing by Neisseria meningitidis Cas9 in vivo. *Genome Biol.*, **19**, 137.
70. Nelson,C.E., Hakim,C.H., Ousterout,D.G., Thakore,P.I., Moreb,E.A., Castellanos Rivera,R.M., Madhavan,S., Pan,X., Ran,F.A., Yan,W.X. *et al.* (2016) In vivo genome editing improves muscle function in a mouse model of Duchenne muscular dystrophy. *Science*, **351**, 403–407.
71. Long,C., McAnally,J.R., Shelton,J.M., Mireault,A.A., Bassel-Duby,R. and Olson,E.N. (2014) Prevention of muscular dystrophy in mice by CRISPR/Cas9-mediated editing of germline DNA. *Science*, **345**, 1184–1188.
72. Amoasii,L., Hildyard,J.C.W., Li,H., Sanchez-Ortiz,E., Mireault,A., Caballero,D., Harron,R., Stathopoulou,T.R., Massey,C., Shelton,J.M. *et al.* (2018) Gene editing restores dystrophin expression in a canine model of Duchenne muscular dystrophy. *Science*, **362**, 86–91.
73. Min,Y.L., Bassel-Duby,R. and Olson,E.N. (2018) CRISPR correction of duchenne muscular dystrophy. *Annu. Rev. Med.*, **70**, 239–255.
74. Singh,K., Evens,H., Nair,N., Rincon,M.Y., Sarcar,S., Samara-Kuko,E., Chuah,M.K. and VandenDriessche,T. (2018) Efficient in vivo Liver-Directed gene editing using CRISPR/Cas9. *Mol. Ther.*, **26**, 1241–1254.
75. Ludwig,N., Leidinger,P., Becker,K., Backes,C., Fehlmann,T., Pallasch,C., Rheinheimer,S., Meder,B., Stahler,C., Meese,E. *et al.* (2016) Distribution of miRNA expression across human tissues. *Nucleic Acids Res.*, **44**, 3865–3877.
76. Baskerville,S. and Bartel,D.P. (2005) Microarray profiling of microRNAs reveals frequent coexpression with neighboring miRNAs and host genes. *RNA*, **11**, 241–247.
77. Chen,C.Z., Li,L., Lodish,H.F. and Bartel,D.P. (2004) MicroRNAs modulate hematopoietic lineage differentiation. *Science*, **303**, 83–86.
78. Jovičić,A., Roshan,R., Moisoi,N., Pradervand,S., Moser,R., Pillai,B. and Luthi-Carter,R. (2013) Comprehensive expression analyses of neural Cell-Type-Specific miRNAs identify new determinants of the specification and maintenance of neuronal phenotypes. *J. Neurosci.*, **33**, 5127–5137.
79. Kim,I., Jeong,M., Ka,D., Han,M., Kim,N.K., Bae,E. and Suh,J.Y. (2018) Solution structure and dynamics of anti-CRISPR AcrIIA4, the Cas9 inhibitor. *Sci. Rep.*, **8**, 3883.
80. Lee,J., Mir,A., Edraki,A., Garcia,B., Amrani,N., Lou,H.E., Gainetdinov,I., Pawluk,A., Ibraheim,R., Gao,X.D. *et al.* (2018) Potent Cas9 inhibition in bacterial and human cells by AcrIIC4 and AcrIIC5 Anti-CRISPR proteins. *MBio.*, **9**, e02321-18.
81. Qin,J.Y., Zhang,L., Clift,K.L., Hulur,I., Xiang,A.P., Ren,B.Z. and Lahn,B.T. (2010) Systematic comparison of constitutive promoters and the doxycycline-inducible promoter. *PLoS One*, **5**, e10611.
82. Weinmann,J. and Grimm,D. (2017) Next-generation AAV vectors for clinical use: an ever-accelerating race. *Virus Genes*, **53**, 707–713.
83. Bengtsson,N.E., Hall,J.K., Odom,G.L., Phelps,M.P., Andrus,C.R., Hawkins,R.D., Hauschka,S.D., Chamberlain,J.R. and Chamberlain,J.S. (2017) Muscle-specific CRISPR/Cas9 dystrophin gene editing ameliorates pathophysiology in a mouse model for Duchenne muscular dystrophy. *Nat. Commun.*, **8**, 14454.
84. Dashkoff,J., Lerner,E.P., Truong,N., Klickstein,J.A., Fan,Z., Mu,D., Maguire,C.A., Hyman,B.T. and Hudry,E. (2016) Tailored transgene expression to specific cell types in the central nervous system after peripheral injection with AAV9. *Mol. Ther. Methods Clin. Dev.*, **3**, 16081.
85. Oakes,B.L., Nadler,D.C., Flamholz,A., Fellmann,C., Staahl,B.T., Doudna,J.A. and Savage,D.F. (2016) Profiling of engineering hotspots identifies an allosteric CRISPR–Cas9 switch. *Nat. Biotechnol.*, **34**, 646–651.
86. Liu,K.I., Ramli,M.N., Woo,C.W., Wang,Y., Zhao,T., Zhang,X., Yim,G.R., Chong,B.Y., Gowher,A., Chua,M.Z. *et al.* (2016) A chemical-inducible CRISPR–Cas9 system for rapid control of genome editing. *Nat. Chem. Biol.*, **12**, 980–987.
87. Polstein,L.R. and Gersbach,C.A. (2015) A light-inducible CRISPR–Cas9 system for control of endogenous gene activation. *Nat. Chem. Biol.*, **11**, 198–200.
88. Nihongaki,Y., Yamamoto,S., Kawano,F., Suzuki,H. and Sato,M. (2015) CRISPR–Cas9-based photoactivatable transcription system. *Chem. Biol.*, **22**, 169–174.
89. Petris,G., Casini,A., Montagna,C., Lorenzin,F., Prandi,D., Romanel,A., Zasso,J., Conti,L., Demichelis,F. and Cereseto,A. (2017) Hit and go CAS9 delivered through a lentiviral based self-limiting circuit. *Nat. Commun.*, **8**, 15334.